Soliton metamorphosis dynamics in ultrafast fiber lasers

Zhiwen He,[1] Yueqing Du,[1] Chao Zeng,[1] Biqiang Jiang,[1] Dong Mao,[1,*] Zhipei Sun,[2] and Jianlin Zhao[1]
[1]*MOE Key Laboratory of Material Physics and Chemistry under Extraordinary Conditions, and Shaanxi Key Laboratory of Optical Information Technology, School of Physical Science and Technology, Northwestern Polytechnical University, Xi'an 710129, China*
[2]*Department of Electronics and Nanoengineering and QTF Centre of Excellence, Aalto University, FI-02150 Aalto, Finland*

(Received 15 December 2020; accepted 22 April 2021; published 17 May 2021)

The transitions from the incoherent noise to the coherent soliton have been fully revealed in ultrafast lasers. However, the soliton transformation between different coherent states, termed as soliton metamorphosis, remains an attractive yet uncharted territory. Here, we reveal the ultrafast dynamics of the soliton metamorphosis via single-shot spectroscopy in a specially designed fiber laser capable of emitting fast-switchable dissipative solitons and stretched pulses. It is demonstrated that the soliton metamorphosis is a consecutive evolution process including the self-phase modulation stage, pulse split stage, and transient stretched pulse stage. Particularly, the long-period pulse breathing and the spectral period doubling appear in the forepart and middle part of the last stage. The metamorphosis dynamics and soliton properties are substantiated by numerical simulation based on a three-step model. This work not only unveils the transient evolution physics of the pulse in soliton metamorphosis, but also provides a simple and effective way to control operations of ultrafast lasers.

DOI: 10.1103/PhysRevA.103.053516

I. INTRODUCTION

The soliton, a term referring to localized structures with high robustness in nonlinear systems, has been universally investigated in numerous fields, including hydrodynamics [1], biomedicines [2], Bose-Einstein condensates [3], optical networks [4], and plasmas [5]. In nonlinear optics, fiber lasers can serve as an ideal platform for exploring new types of solitons and unveiling their underlying dynamics. Via engineering the dispersion and nonlinearity of a cavity, fiber lasers have successfully delivered conventional solitons [6], stretched pulses (SPs) [7], self-similar solitons [8], and dissipative solitons (DSs) [9]. Among them, SPs, also known as dispersion-managed solitons, are formed in the near-zero dispersion regime where pulses experience significant broadening and compression along the cavity, thus enabling the bandwidth and duration to be tens of nanometers and sub-100 fs, respectively [10,11]. DSs arise from the balance of gain and loss in the presence of normal dispersion and strong nonlinearity, typically featuring giant frequency chirps and quasirectangular spectra [12]. SPs and DSs are distinct attractors [12] with a considerable distance in the phase space of the nonlinear-dissipative system, which is difficult to mutually transform by simply changing one operation parameter.

The soliton buildup dynamics in mode-locked lasers have attracted substantial attention [13,14] in the research community since continuous evolutions of pulses were recorded through streak-camera systems in the 1970s [15]. Simultaneously, numerous works were focused on pulse evolution in steady mode-locked states, revealing the multisoliton mode-locking dynamics [16], critical behavior of light [17], and the vector nature of the soliton [18] in fiber lasers. Recently, the dispersive Fourier transform (DFT) technique, capable of mapping the spectral information into the temporal domain with dispersive elements, has been applied to reveal transient dynamics including beating and relaxation oscillation in the buildup process from noises to coherent solitons [19], and phase drift during the interaction or dissociation of soliton molecules [20–22] in the stable mode-locking state. By tuning the polarization state with an electric polarization controller, the transition dynamics from narrow-spectrum to wide-spectrum pulses were also disclosed in a nonlinear polarization rotation mode-locked laser [23]. The aforementioned works mainly focused on the formation and evolution of single-type solitons, while the transformation between different types of coherent solitons remains an uncharted regime, which is also vital for both understanding underlying soliton dynamics and controlling laser operations.

In this paper, we demonstrate a fiber ring laser that is capable of emitting DSs at 1570 nm and SPs at 1590 nm based on chromatic dispersion of erbium-doped fiber (EDF) and nonlinear transmission of saturable absorber. Simulations substantiate the experiments and confirm that the elevation of pump power is directly responsible for the metamorphic change of pulses. With the DFT technique, the soliton transformation dynamics are disclosed in real time, which can be a consecutive process including three evolution stages, namely, self-phase modulation, pulse split, and transient SP. Such phenomenon is termed as soliton metamorphosis to picturesquely depict the continuous transformation process between different types of ultrashort pulses.

II. EXPERIMENTAL SETUP AND PRINCIPLE

The configuration of the fiber laser and measurement system is shown in Fig. 1(a). The laser diode (LD) pumps the 4-m EDF (Nufern: EDFL-980-HP) via a 980/1550 nm wavelength division multiplexer (WDM), and the optical coupler

*maodong@nwpu.edu.cn

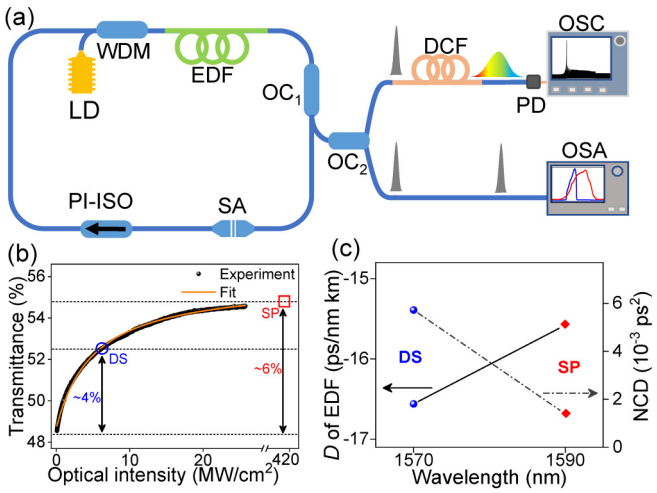

FIG. 1. Experimental setup and operation principle of the fiber laser. (a) Configuration of the fiber laser and measurement system. (b) Nonlinear transmission property of the carbon nanotube saturable absorber, for the DS and SP operations; the transmissions are unequal with a difference of 2%. (c) Wavelength-dependent dispersions of EDF and cavity, enabling the transformation from the DS to SP. LD, laser diode; WDM, wavelength division multiplexer; EDF, erbium-doped fiber; OC, output coupler; SA, saturable-absorber; PI-ISO, polarization-insensitive isolator; DCF, dispersion compensation fiber; PD, photodetector; OSC, oscilloscope; OSA, optical spectrum analyzer; DS, dissipative soliton; SP, stretched pulse; NCD, net cavity dispersion.

(OC) outputs a 20% laser. The carbon nanotube saturable absorber (CNT SA) enables the passive mode locking. The polarization-insensitive isolator (PI-ISO) guarantees the unidirectional propagation of pulses. All other fiber components are made of single-mode fiber (SMF, Corning: SMF-28e+) with a total length of ∼3.6 m. For the DFT measurement, the output pulses are broadened by a 2000-m dispersion compensation fiber (total group velocity dispersion: ∼387 ps^2) to transform their spectral profiles into temporal waveforms. Subsequently, a 5-GHz photodetector and a 4-GHz oscilloscope are used to capture the broadened pulses. The spectral resolution of the DFT system is calculated as ∼0.83 nm [24], sufficient for the spectra to be measured.

In this scheme, the laser can be switched from DS to SP states by elevating the pump power. As the pump power reaches 9.3 mW, a continuous wave located at 1570 nm emerges in the proposed fiber laser. When the pump power ranges from 10.1 to 15.4 mW, the laser emits DSs centered at 1570 nm. Interestingly, when the pump power exceeds 15.5 mW, the laser evolves into the SP operation, and the central wavelength shifts to 1590 nm. The stable SP operation can be maintained in the fiber laser when the pump power enlarges from 15.5 to 36.5 mW. Such phenomenon is repeatable by tuning the pump power, which is indeed induced by the nonlinear transmission of SA and the chromatic dispersion of the gain medium.

As shown in Fig. 1(b), the nonlinear transmittance (T) of the CNT SA is fitted by a common model [25,26]:

$$T = (1 - \alpha_{ns}) - \frac{\alpha_s}{1 + I/I_s}, \quad (1)$$

where I denotes the incident optical intensity, I_s represents the saturable optical intensity, α_s is the modulation depth, and α_{ns} is the nonsaturable absorption component. The modulation depth and saturable optical intensity of the CNT SA are ∼6% and ∼25 MW/cm^2, respectively. In the experiment, the optical intensities of DSs and SPs inside the cavity are calculated to be ∼6 and ∼410 MW/cm^2, as marked by the blue circle and red square. Evidently, the saturable absorber is not saturated with a transmittance of ∼52.5% for DS operation, while it becomes fully saturated with a transmittance of ∼54.5% for SP operation.

Therefore, under a pump power of 12 mW, the CNT SA is not fully saturated, which introduces a larger nonsaturable loss and the laser emits DSs centered at 1570 nm. By contrast, the intracavity pulse intensity reaches the saturable optical intensity through increasing the pump power to 17.5 mW; thus the SA becomes fully saturated with a lower loss and the lasing wavelength shifts to 1590 nm because of the wavelength-dependent gain coefficient of EDF [27]. Such phenomenon coincides with the previous reports that the lasing wavelength moves towards the red side for a smaller intracavity loss [28]. As the dispersion parameter D of the EDF varies with wavelength (e.g., −16.5 ps/(nm km) at 1570 nm and −15.5 ps/(nm km) at 1590 nm), the net cavity dispersion (NCD) declines from the positive to the near-zero regime [Fig. 1(c)], which contributes to the soliton metamorphosis from DS to SP.

III. EXPERIMENTAL AND SIMULATION RESULTS OF DS AND SP

Figures 2(a) and 2(b) show the typical spectra and autocorrelation traces of measured pulses operating at the DS and SP regimes. The DS centered at 1570 nm exhibits the characteristic quasirectangular spectrum with a 3-dB bandwidth of ∼17 nm, while the SP centered at 1590 nm displays a broad spectrum with a bandwidth of ∼38 nm [Fig. 2(a)]. The measured spectra are slightly asymmetrical, which could be attributed to the uneven gain spectrum of EDF [11]. The weak pedestal on the DS spectrum results from the amplified spontaneous emission of the EDF. The durations of DS and SP are ∼3.3 ps and 125 fs using the Gaussian fit [Fig. 2(b)], which give the time-bandwidth products of ∼6.83 and 0.55, respectively. For both operations, only a single pulse circulates inside the cavity with a period of 37.2 ns. Due to the chromatic dispersion of the cavity, the group velocities of the DS and SP are slightly different, resulting in a deviation of 33 Hz between their fundamental repetition rates (see Appendix A).

Based on the lumped propagation model in which discrete fiber components of the cavity are modeled by separated transmission functions, numerical simulations are performed by solving the nonlinear Schrödinger equation [29] that incorporates the dispersion, nonlinearity, gain, and loss of fibers:

$$\frac{\partial u}{\partial z} = -i\frac{\beta_2}{2}\frac{\partial^2 u}{\partial t^2} + \frac{g - l}{2}u + i\gamma|u|^2 u + \frac{g}{2\Omega_g^2}\frac{\partial^2 u}{\partial t^2}, \quad (2)$$

where u is the slowly varying envelope of the pulse propagating in fibers, and z and t represent the cavity position

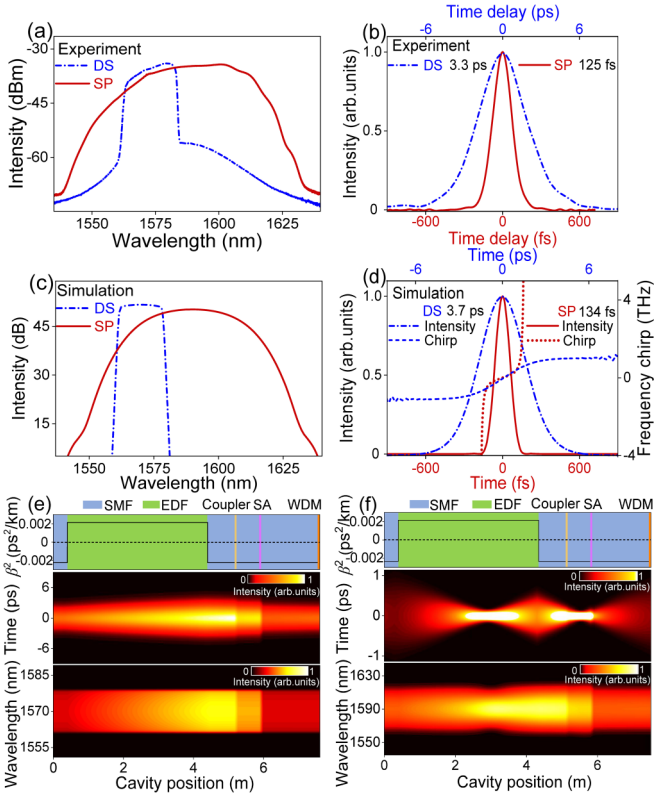

FIG. 2. Experiment and simulation results of the DS and SP formed in the same laser. (a) Measured spectra, and (b) autocorrelation traces. (c) Simulation spectra, and (d) pulse intensities and frequency chirps. The intensities of DS and SP are denoted by blue (short dash dot) and deep red (solid) curves, while the frequency chirps of DS and SP are delineated by blue (short dash) and red (short dot) curves, respectively. Intracavity dispersion map (top panel), temporal evolution (middle panel), and spectral evolution (bottom panel) for (e) DS and (f) SP.

and the time coordinate respectively. Ω_g denotes the gain spectrum of EDF and l is the loss of fibers. β_2 and γ are the second-order dispersion coefficient and cubic refractive nonlinearity of fibers, respectively. The gain of EDF is expressed as $g = g_0 \exp(-E_p/E_s)$, where g_0, E_p, and E_s are the small-signal gain coefficient, pulse energy, and gain saturation energy, respectively. The transfer function $T = 0.49 - T_0/[1 - P_{(\tau)}/P_{sat}]$ is used to model the saturable absorber, where T denotes the transmission, T_0 is the modulation depth, $P_{(\tau)}$ is the instantaneous pulse power, and P_{sat} is the saturation power. $\Omega_g = 25\,\text{nm}$, $g_0 = 0.7\,\text{m}^{-1}$, $T_0 = 6\%$, $P_{sat} = 20\,\text{W}$, $\gamma = 4.2\,\text{W}^{-1}\,\text{km}^{-1}$ for EDF and $\gamma = 1.3\,\text{W}^{-1}\,\text{km}^{-1}$ for SMF. For the DS operation at 1570 nm, $\beta_2 = 21.5\,\text{ps}^2/\text{km}$ for EDF and $-22.3\,\text{ps}^2/\text{km}$ for SMF ($\beta_2 = -\lambda^2 D/2\pi c$, λ is wavelength, D is dispersion parameter, and c is speed of light in vacuum), and $E_s = 23\,\text{pJ}$. For the SP operation at 1590 nm, $\beta_2 = 20.8\,\text{ps}^2/\text{km}$ for EDF and $-22.8\,\text{ps}^2/\text{km}$ for SMF, and $E_s = 35\,\text{pJ}$.

The saturation energy and dispersion parameter, respectively related to the pump power and cavity dispersion, change accordingly for DS and SP operations, while the other parameters are fixed. As displayed in Figs. 2(c) and 2(d), the bandwidth of the simulated DS/SP is ∼17/37 nm, and the pulse duration of the simulated DS/SP is ∼3.7 ps/134 fs. The evolutions of DS and SP versus cavity positions are shown in Figs. 2(e) and 2(f), in which the duration of the DS ranges from ∼2.9 to 4 ps while the bandwidth remains almost constant. In contrast, the SP breathes twice from 130 fs to 1.44 ps with a ratio of ∼11, indicating that the dispersion and the nonlinearity are not balanced locally along the cavity [30]. Simulation results well reproduce the experimental observations, which corroborate the operation principle. As the Haus master equation approach assumes an average dispersion value and a small change of pulse per pass [31], DSs are obtained while the SPs cannot be achieved with this simulation method. Apparently, the DS and SP are intrinsically distinct from each other in aspects of pulse properties, as well as the formation and evolution mechanisms. Thus, the transformation from DS to SP can be regarded as a typical type of soliton metamorphosis in the version of optics.

IV. SOLITON METAMORPHOSIS DYNAMICS FROM DS TO SP

The dynamics of soliton metamorphosis from giant-chirp DS to chirp-free SP are revealed in real time via the DFT technique. For both pulses, the waveforms recorded by the oscilloscope are consistent with the time-averaged spectra captured by the optical spectrum analyzer (see Appendix B), validating the reliability of the DFT system. The data series are segmented with respect to the cavity round-trip (RT) time, and manifested as a two-dimensional graph where the horizontal axis shows the consecutive RT number, the vertical axis denotes the wavelength, and the color scale represents the normalized spectral intensity [Fig. 3(a)]. The Fourier transformation of the single-shot spectrum—field autocorrelation trace [32]—is plotted to study the temporal evolution of pulses [Fig. 3(b)].

The whole soliton metamorphosis, lasting for ∼0.133 ms or ∼3590 RTs, is a consecutive process composed of three distinct stages—self-phase modulation, pulse split, and transient SP (a complex process including the unstable state, the pulse breathing behavior, and the pulse pulsating phenomenon). As demonstrated in Figs. 3(a) and 3(b), the fiber laser initially delivers a stable DS, and its spectrum starts to broaden and shifts towards a longer wavelength after elevating the pump power. In the normal dispersion regime, the initial pulse can sustain high nonlinearity due to its relatively large duration; hence the fiber laser keeps emitting DSs with higher intensity for the next 580 RTs, instead of directly evolving to the SP state. In this stage, the higher pump reinforces the self-phase modulation effect and plays a dominant role, as evidenced by the spectral fringes in Fig. 3(c) and the temporal pedestals in Fig. 3(d). After that, the transmission of SA increases as the pulse intensity reaches the peak value [Fig. 1(b)]. Simultaneously, the lasing wavelength shifts to a longer wavelength and the NCD reaches the near-zero regime, due to nonlinear absorption of SA and chromatic dispersion of fibers [Fig. 1(c)].

Confined by the effective gain bandwidth [33], the pulse then splits into two unequal parts that separate from each other and reach the maximum separation of ∼2.2 ps from ∼580 to ∼630 RTs, as indicated by the spectral interference patterns in Fig. 3(c) and the nascent pulse in Fig. 3(d). As

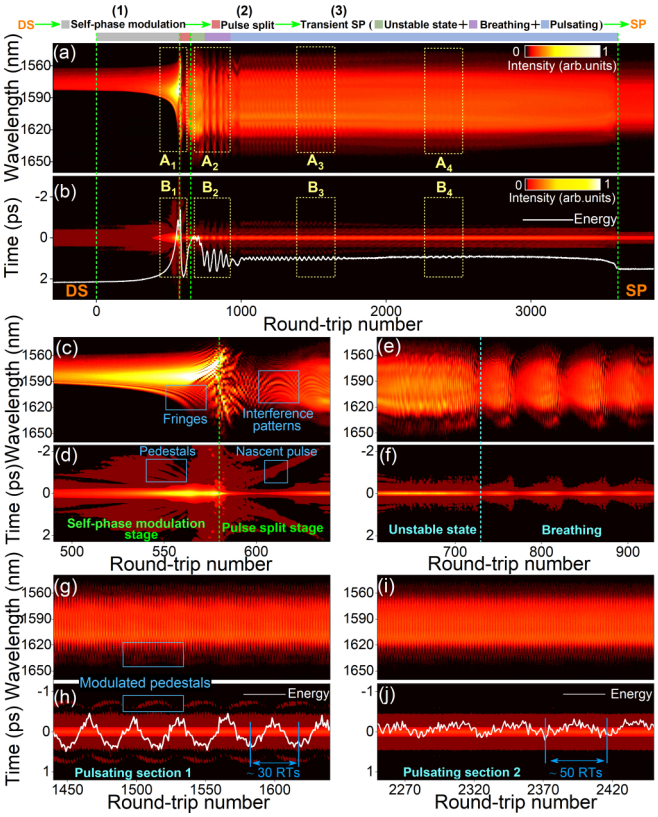

FIG. 3. Spectra, field autocorrelation traces, and energy evolutions of the soliton metamorphosis. Top panel: three typical stages in the transformation process. (a), (b) Whole evolution process. (c), (d) (Expanded regions A_1, B_1) Self-phase modulation stage and pulse split stage. Transient SP stage: (e), (f) (expanded regions A_2, B_2) unstable state and breathing state; (g)–(j) (expanded regions A_3, B_3 and A_4, B_4) pulse pulsating sections 1 and 2.

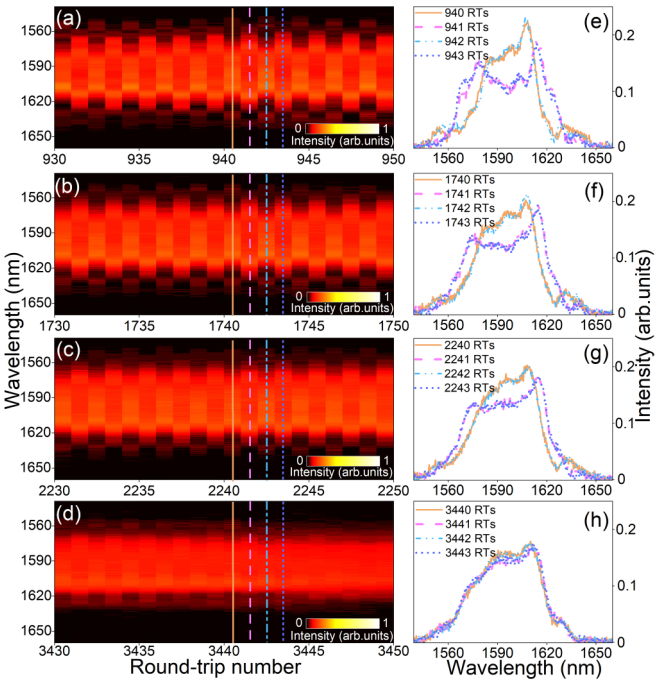

FIG. 4. Spectral period doubling phenomena in the pulsating state. (a)–(d) Spectral evolutions over 20 RTs, and (e)–(h) representative spectra over 4 RTs of period doubling pulses. Adjacent spectra are denoted by yellow (solid), magenta (dash), light blue (dash dot dot), and navy blue (short dot) curves, respectively.

the SA and gain competition suppress the lower-intensity components, known as the "strongest pulse survive law" [34], the weaker pulse vanishes and the lasing wave evolves to the single-pulse state at ~630 RTs. Subsequently, it comes into the complex transient SP stage comprising the unstable state, the breathing, and the pulsating of the pulse. In the unstable state, the high-intensity pulse displays an obvious instability from ~630 to ~750 RTs, where the spectral and temporal profiles evolve erratically due to the strong fiber nonlinearity that further destabilizes the self-consistent evolution of intracavity pulses [left side of Figs. 3(e) and 3(f)]. Then, the unstable pulse evolves to the breathing state (~750 to ~930 RTs) that consists of four similar spectral variations with the period of ~45 RTs and spectral breathing ratio of ~1.9 [right side of Figs. 3(e) and 3(f)]. Such breathing phenomenon is intrinsically arisen from the competition between the gain and loss, usually triggered by the variation of the pump power [35].

The pulse evolves into a long pulsating state from ~930 to ~3580 RTs, where the energy oscillations accompanied by spectral or temporal modulated pedestals appear twice (section 1: from ~980 to ~1750 RTs with a period of 30 RTs; section 2: from ~2130 to ~2630 RTs with a period of 50 RTs), as illustrated in Figs. 3(g)–3(j). Energy oscillation is a characteristic behavior of soliton pulsation [36,37], but there are some exceptions; e.g., the "invisible soliton pulsation" exhibits the invariable pulse energy [38]. Then, the intensity, bandwidth, and duration of the pulse suddenly decline from ~3580 to ~3590 RTs and the laser finally reaches the stable SP mode-locking state. The process of the soliton metamorphosis is further displayed in the movie in the Supplemental Material [39], where the DS evolves consecutively to SP.

Such soliton metamorphosis is a repeatable physical process with similar evolution dynamics. Another group of the soliton metamorphosis is displayed in Appendix C, which also contains the self-phase modulation stage, the pulse split stage, and the transient SP stage. However, there are some tiny differences between the two evolutions, for example, in the transient SP stage, the breathing period is constant in Fig. 3 while it changes obviously in Appendix C. Unlike the discontinuous transformation between single-type pulses in the nonlinear polarization rotation mode-locked laser [23], the soliton metamorphosis represents a consecutive transformation process between two distinct types of pulses, which can be ascribed to the polarization-insensitive saturable absorption property of CNT SA that is capable of maintaining various ultrashort solitons.

Interestingly, the spectral period doubling of the pulse emerges in a damping style over the whole pulsating state. Figures 4(a)–4(h) display the four consecutive spectral evolutions at different regions, and the labels correspond to their RT numbers. Obviously, two pulses with different spectra show up every two RTs (concave at odd RTs while smooth at even RTs), indicating a repetitive energy redistribution between the spectral edges and centers. A similar phenomenon is reproduced in the other soliton metamorphosis (see Appendix C)

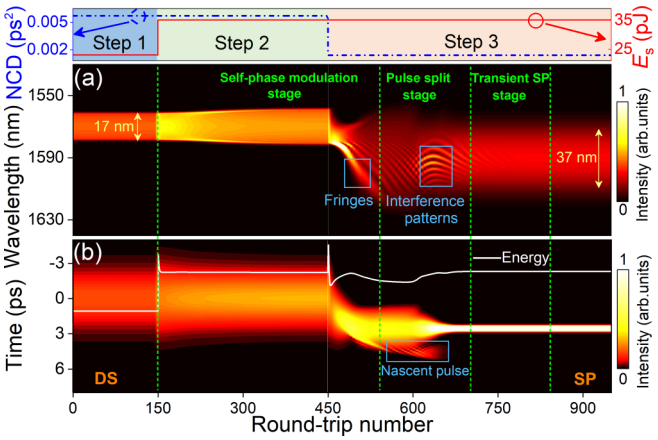

FIG. 5. Simulation of soliton metamorphosis from DS to SP. Top panel: sketch of the three-step model; the NCD and E_s of the laser are denoted by blue (short dash dot) and red (solid) lines. (a) Spectral and (b) temporal evolutions. NCD: net cavity dispersion; E_s: gain saturation energy.

and has also been reported in the buildup process of conventional solitons [40], which can be attributed to the instability caused by the self-phase modulation effect. Although adjacent spectra are quite different in the forepart of the pulsating state, they gradually evolve into the same steady state. The present results confirm that the spectral period doubling is a universal phenomenon that not only appears in the buildup process of mode locking, but also in the evolution of soliton metamorphosis.

V. THREE-STEP MODEL FOR SOLITON METAMORPHOSIS

We propose a three-step model to describe the metamorphic transformation of solitons, as illustrated in the top panel of Fig. 5. The propagation of the pulse in the fiber is simulated by solving Eq. (2), and parameter settings are identical to those used in Fig. 2. A stable DS centered at 1570 nm is first formed in the fiber laser with the NCD of $\sim$0.0057 ps^2; then it works as the input pulse, and the gain saturation energy is elevated from 23 to 35 pJ to model the increase of the pump power that triggers the soliton metamorphosis. After that, the resulting pulse is injected into the same resonator while the wavelength shifts to 1590 nm and the NCD decreases to $\sim$0.0014 ps^2.

Figures 5(a) and 5(b) show the spectral and temporal evolutions of the simulated pulse versus the RT number. Similar to the experimental observations in Fig. 3, the pulse undergoes a consecutive transformation process comprising self-phase modulation stage, pulse split stage, and transient SP stage. In the self-phase modulation stage, due to the enhancement of the gain saturation energy, the spectrum broadens slightly in the forepart, while the pulse energy exhibits a strong shake when the NCD is reduced to the near-zero regime. Then, accompanied by the redshift of the center wavelength, the spectrum is stretched drastically and displays a series of spectral fringes caused by the self-phase modulation effect. After that, the spectral interference patterns appear and the pulse splits into two unequal parts (the nascent pulse exists for tens of RTs), which are consistent with the experiment results in Figs. 3(c) and 3(d). Subsequently, the pulse enters into the transient SP stage, where the spectrum and pulse gradually evolve from the unstable state to the self-consistent steady state. It is apparent that the overall evolution, spectral fringes, interference patterns, and nascent pulse in the simulation coincide with those of the experiment, further confirming the authenticity of the proposed model.

In contrast to the transitions from the incoherent noise to the coherent soliton [19] or the formation of soliton molecules [34], the reproducible soliton metamorphosis depicts a unique transformation process between two distinct types of coherent pulses. It is possible to explore other transient phenomena via manipulating the operation parameters in the process of soliton metamorphosis, as confirmed by the interesting phenomena in the transient SP stage of Appendix C.

VI. CONCLUSIONS

In conclusion, by virtue of the wavelength-sensitive chromatic dispersion of the gain medium and the nonlinear transmission of SA, we achieve a mode-locked fiber laser that emits fast-switchable DSs and SPs via controlling the pump power. Our study reveals the underlying dynamics of the soliton metamorphosis from DS to SP, which contributes to a deeper understanding of soliton evolution and therefore improves the controllability of ultrafast lasers. Besides the DSs and SPs, fiber lasers also support the generation of conventional solitons [6], self-similar solitons [8], and noise-like pulses [41]; therefore the soliton metamorphosis between other types of pulses remains an interesting while unexplored issue in nonlinear optics. Additionally, the dynamics of the soliton metamorphosis could be qualitatively substantiated by the nonlinear Schrödinger equation that was also utilized to interpret nonlinear phenomena in oceanography [42], Bose-Einstein condensation [43], and plasma [5]. Consequently, it is natural to hypothesize soliton metamorphosis as a universal concept that may be extended to the aforementioned fields.

ACKNOWLEDGMENTS

This work was supported by the National Key R&D Program of China (Grant No. 2017YFA0303800), the National Natural Science Foundation of China (Grants No. 11634010 and No. 11874300), and the Fundamental Research Funds for

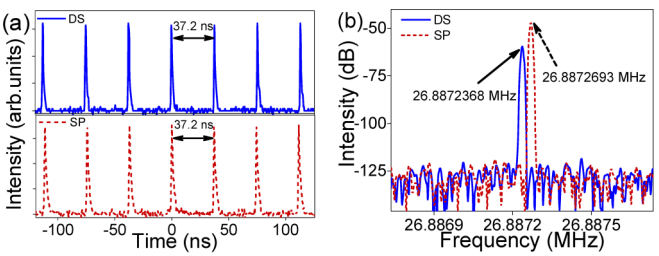

FIG. 6. (a) Oscilloscope traces and (b) radio frequency spectra of the DS and SP. The DS and SP are denoted by blue (solid) and deep red (short dash) curves, respectively. The adjacent pulse separations for both DS and SP are about 37.2 ns, and the difference between two fundamental repetition rates is 33 Hz.

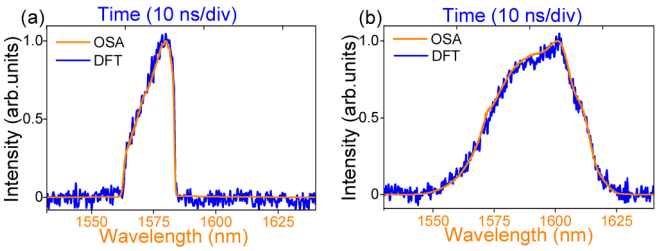

FIG. 7. Validity of the DFT technique. Comparison between the single-shot spectra captured by dispersive Fourier transform technique (blue curves) and time-averaged spectra obtained via optical spectrum analyzer (orange curves). (a) DS and (b) SP.

the Central Universities (Grants No. 3102019JC008 and No. 3102019PY002).

APPENDIX A: OSCILLOSCOPE TRACES AND RADIO FREQUENCY SPECTRA OF THE DS AND SP

Figure 6(a) depicts the oscilloscope traces of the DS and SP, and both of them have the same pulse-pulse separation of ∼37.2 ns, which coincides with the cavity length of ∼7.6 m.

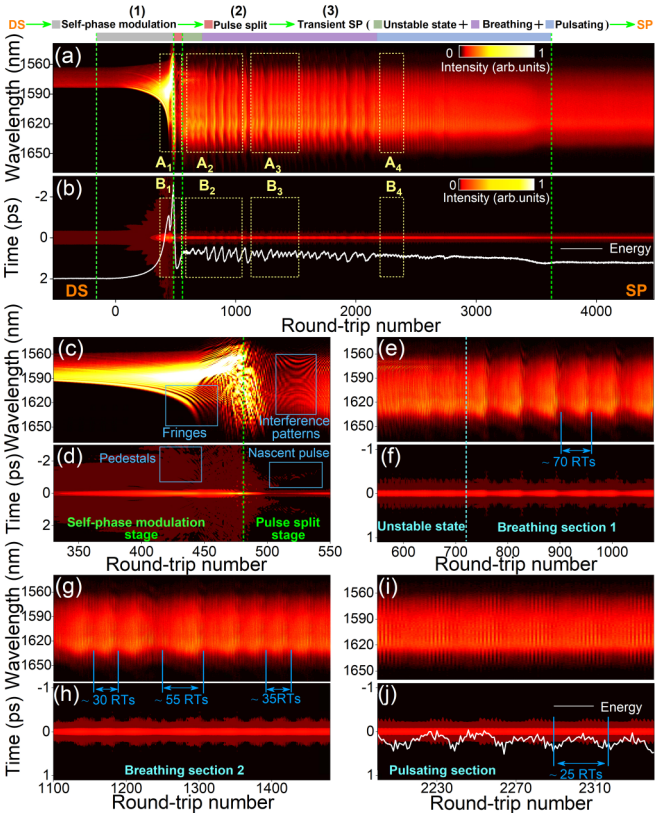

FIG. 8. Spectra, field autocorrelation traces, and energy evolutions for another group of soliton metamorphosis. Top panel: three typical stages in the transformation process. (a), (b) Spectra and field autocorrelation traces of the whole process. (c), (d) (Expanded regions A_1, B_1) Self-phase modulation stage and pulse split stage. Transient SP stage: (e), (f) (expanded regions A_2, B_2) unstable state and breathing section 1; (g), (h) (expanded regions A_3, B_3) breathing section 2; (i), (j) (expanded regions A_4, B_4) pulse pulsating section.

The radio-frequency spectra are delineated in Fig. 6(b), giving the fundamental repetition rates of 26.887 236 8 MHz and 26.887 269 3 MHz for DS and SP, respectively. The small deviation on the radio-frequency spectra can be ascribed to the slightly different group velocities, and the high signal to noise ratios (>60 dB) verify the good stability of both the DS and SP.

APPENDIX B: VALIDITY OF THE DFT TECHNIQUE

As displayed in Figs. 7(a) and 7(b), after propagating through a 2000-m dispersion compensation fiber (DCF), the full width at half maxima of DS and SP approached ∼6.6 and ∼13.6 ns respectively, coinciding well with the DFT mapping relation [24]:

$$\Delta t = |D|L\Delta\lambda, \tag{B1}$$

where Δt relates to the full width at half maximum of the broadened pulse, and $\Delta\lambda$ corresponds to the 3-dB bandwidth of the time-averaged spectrum. D [–150 ps/(nm km)] and L (2000 m) are the dispersion parameter and length of DCF, respectively. According to the final limitation of the DFT technique [24], the spectral resolution is calculated to be 0.83 nm, which is sufficient for resolving the spectra to be measured. Besides, for both DS and SP, the single-shot spectra exhibit similar profiles as the time-averaged linear spectra, also validating the reliability of the DFT measurement system.

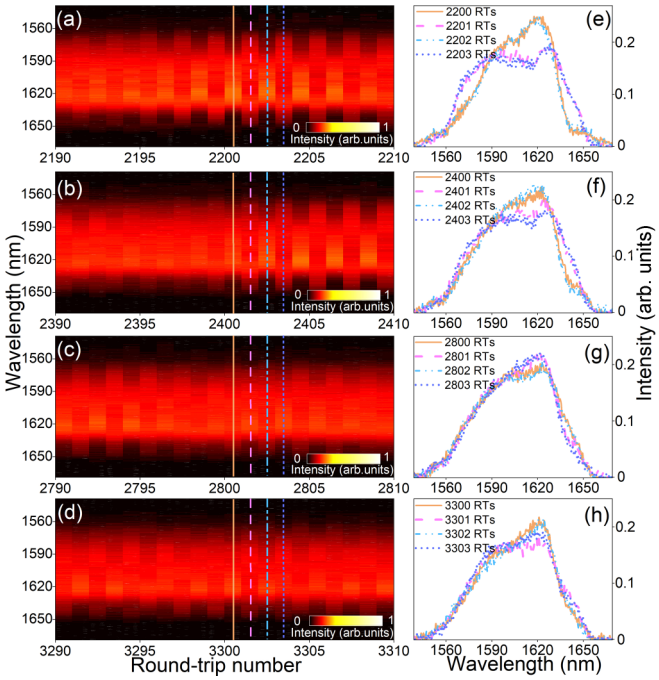

FIG. 9. Spectral period doubling phenomena in the pulsating state for another soliton metamorphosis. (a)–(d) Spectral evolutions over 20 RTs, and (e)–(h) representative spectra over 4 RTs of period doubling pulses. Adjacent spectra are denoted by yellow (solid), magenta (dash), light blue (dash dot dot), and navy blue (short dot) curves, respectively.

APPENDIX C: REPRODUCIBILITY OF THE SOLITON METAMORPHOSIS

The soliton metamorphosis is a repeatable physical process that exhibits similar evolution dynamics. Figure 8 shows another group of soliton metamorphosis under the same experiment conditions as that of Fig. 3 in the main text. The whole soliton metamorphosis, lasting for ∼0.131 ms or ∼3530 RTs, is also a consecutive process composed of a similar self-phase modulation stage, pulse split stage, and transient SP stage. However, there are some tiny differences between the two evolution dynamics; for example, in the transient SP stage, the breathing period is constant in Fig. 3 of the main text while it changes obviously in Fig. 8.

Interestingly, the spectral period doubling is also reproduced in this soliton metamorphosis, as illustrated in Fig. 9. Similar to the result in Fig. 4 of the main text, the adjacent spectra are quite different in the forepart of the pulsating state, and they gradually evolve into the same steady state. Our results confirm that the spectral period doubling is a universal phenomenon that not only appears in the buildup process of mode locking but also in the evolution of the soliton metamorphosis.

[1] J. Wu, R. Keolian, and I. Rudnick, Observation of a Nonpropagating Hydrodynamic Soliton, Phys. Rev. Lett. **52**, 1421 (1984).

[2] A. S. Davydov, Solitons and energy transfer along protein molecules, J. Theor. Biol. **66**, 379 (1977).

[3] Y. V. Kartashov and V. V. Konotop, Solitons in Bose-Einstein Condensates with Helicoidal Spin-Orbit Coupling, Phys. Rev. Lett. **118**, 190401 (2017).

[4] F. M. Knox, W. Forysiak, and N. J. Doran, 10-Gbit/s soliton communication systems over standard fiber at 1.55 μm and the use of dispersion compensation, J. Lightwave Technol. **13**, 1955 (1995).

[5] N. J. Zabusky and M. D. Kruskal, Interaction of "Solitons" in a Collisionless Plasma and the Recurrence of Initial States, Phys. Rev. Lett. **15**, 240 (1965).

[6] S. J. Beecher, R. R. Thomson, N. D. Psaila, Z. Sun, T. Hasan, A. G. Rozhin, A. C. Ferrari, and A. K. Kar, 320 fs pulse generation from an ultrafast laser inscribed waveguide laser mode-locked by a nanotube saturable absorber, Appl. Phys. Lett. **97**, 111114 (2010).

[7] K. Tamura, E. P. Ippen, H. A. Haus, and L. E. Nelson, 77-fs pulse generation from a stretched-pulse mode-locked all-fiber ring laser, Opt. Lett. **18**, 1080 (1993).

[8] B. Oktem, C. Ülgüdür, and F. Ö. Ilday, Soliton–similariton fibre laser, Nat. Photonics **4**, 307 (2010).

[9] L. M. Zhao, D. Y. Tang, and J. Wu, Gain-guided soliton in a positive group-dispersion fiber laser, Opt. Lett. **31**, 1788 (2006).

[10] K. Tamura, E. P. Ippen, and H. A. Haus, Pulse dynamics in stretched-pulse fiber lasers, Appl. Phys. Lett. **67**, 158 (1995).

[11] W. He, M. Pang, C. R. Menyuk, and P. St. J. Russell, Sub-100-fs 1.87 GHz mode-locked fiber laser using stretched-soliton effects, Optica **3**, 1366 (2016).

[12] P. Grelu and N. Akhmediev, Dissipative solitons for mode-locked lasers, Nat. Photonics **6**, 84 (2012).

[13] J. C. Kuo and C. L. Pan, Buildup of steady-state subpicosecond and femtosecond pulses in a colliding-pulse mode-locked ring dye laser, Opt. Lett. **15**, 1297 (1990).

[14] J. A. R. Williams, P. M. W. French, and J. R. Taylor, An investigation into femtosecond pulse formation in a continuously-pumped passively-mode-locked CPM ring dye laser, IEEE J. Quantum Electron. **26**, 1434 (1990).

[15] E. G. Arthurs, D. J. Bradley, and A. G. Roddie, Buildup of picosecond pulse generation in passively mode-locked rhodamine dye lasers, Appl. Phys. Lett. **23**, 88 (1973).

[16] R. Weill, B. Vodonos, A. Gordon, O. Gat, and B. Fischer, Statistical light-mode dynamics of multipulse passive mode locking, Phys. Rev. E **76**, 031112 (2007).

[17] R. Weill, A. Rosen, A. Gordon, O. Gat, and B. Fischer, Critical Behavior of Light in Mode-Locked Lasers, Phys. Rev. Lett. **95**, 013903 (2005).

[18] D. Y. Tang, H. Zhang, L. M. Zhao, and X. Wu, Observation of High-Order Polarization-Locked Vector Solitons in a Fiber Laser, Phys. Rev. Lett. **101**, 153904 (2008).

[19] G. Herink, B. Jalali, C. Ropers, and D. R. Solli, Resolving the build-up of femtosecond mode-locking with single-shot spectroscopy at 90 MHz frame rate, Nat. Photonics **10**, 321 (2016).

[20] K. Krupa, K. Nithyanandan, U. Andral, P. Tchofo-Dinda, and P. Grelu, Real-Time Observation of Internal Motion within Ultrafast Dissipative Optical Soliton Molecules, Phys. Rev. Lett. **118**, 243901 (2017).

[21] Z. Q. Wang, K. Nithyanandan, A. Coillet, P. Tchofo-Dinda, and P. Grelu, Optical soliton molecular complexes in a passively mode-locked fibre laser, Nat. Commun. **10**, 830 (2019).

[22] Y. Zhou, Y.-X. Ren, J. Shi, H. Mao, and K. K. Y. Wong, Buildup and dissociation dynamics of dissipative optical soliton molecules, Optica **7**, 965 (2020).

[23] G. Pu, L. Yi, L. Zhang, C. Luo, Z. Li, and W. Hu, Intelligent control of mode-locked femtosecond pulses by time-stretch-assisted real-time spectral analysis, Light Sci. Appl. **9**, 13 (2020).

[24] K. Goda and B. Jalali, Dispersive Fourier transformation for fast continuous single-shot measurements, Nat. Photonics **7**, 102 (2013).

[25] F. Wang, A. G. Rozhin, V. Scardaci, Z. Sun, F. Hennrich, I. H. White, W. I. Milne, and A. C. Ferrari, Wideband-tuneable, nanotube mode-locked, fibre laser, Nat. Nanotechnol. **3**, 738 (2008).

[26] S. B. Lu, L. L. Miao, Z. N. Guo, X. Qi, C. J. Zhao, H. Zhang, S. C. Wen, D. Y. Tang, and D. Y. Fan, Broadband nonlinear optical response in multi-layer black phosphorus: An emerging infrared and mid-infrared optical material, Opt. Express **23**, 11183 (2015).

[27] Y. W. Lee, J. Nilsson, S. T. Hwang, and S. J. Kim, Experimental characterization of a dynamically gain-flattened erbium-doped fiber amplifier, IEEE Photonics Technol. Lett. **8**, 1612 (1996).

[28] Y. Meng, M. Salhi, A. Niang, K. Guesmi, G. Semaan, and F. Sanchez, Mode-locked Er:Yb-doped double-clad fiber laser with 75-nm tuning range, Opt. Lett. **40**, 1153 (2015).

[29] G. P. Agrawal, *Nonlinear Fiber Optics* (Academic Press, New York, 2001).

[30] X. Dong, Q. Yang, C. Spiess, V. G. Bucklew, and W. H. Renninger, Stretched-Pulse Soliton Kerr Resonators, Phys. Rev. Lett. **125**, 033902 (2020).

[31] H. A. Haus, J. G. Fujimoto, and E. P. Ippen, Analytic theory of additive pulse and Kerr lens mode-locking, IEEE J. Quantum Electron. **28**, 2086 (1992).

[32] G. Herink, F. Kurtz, B. Jalali, D. R. Solli, and C. Ropers, Real-time spectral interferometry probes the internal dynamics of femtosecond soliton molecules, Science **356**, 50 (2017).

[33] D. Y. Tang, L. M. Zhao, B. Zhao, and A. Q. Liu, Mechanism of multisoliton formation and soliton energy quantization in passively mode-locked fiber lasers, Phys. Rev. A **72**, 043816 (2005).

[34] X. Liu, X. Yao, and Y. Cui, Real-Time Observation of the Buildup of Soliton Molecules, Phys. Rev. Lett. **121**, 023905 (2018).

[35] J. Peng, S. Boscolo, Z. Zhao, and H. Zeng, Breathing dissipative solitons in mode-locked fiber lasers, Sci. Adv. **5**, eaax1110 (2019).

[36] Y. Du, Z. Xu, and X. Shu, Spatio-spectral dynamics of the pulsating dissipative solitons in a normal-dispersion fiber laser, Opt. Lett. **43**, 3602 (2018).

[37] T. Xian, L. Zhan, W. Wang, and W. Zhang, Subharmonic Entrainment Breather Solitons in Ultrafast Lasers, Phys. Rev. Lett. **125**, 163901 (2020).

[38] M. Liu, Z. W. Wei, H. Li, T. J. Li, A. P. Luo, W. C. Xu, and Z. C. Luo, Visualizing the "invisible" soliton pulsation in an ultrafast laser, Laser Photonics Rev. **14**, 1900317 (2020).

[39] See Supplemental Material at http://link.aps.org/supplemental/10.1103/PhysRevA.103.053516 for a movie displaying the real-time revealing of the soliton metamorphosis from DS to SP.

[40] J. Peng, M. Sorokina, S. Sugavanam, N. Tarasov, D. V. Churkin, S. K. Turitsyn, and H. Zeng, Real-time observation of dissipative soliton formation in nonlinear polarization rotation mode-locked fibre lasers, Commun. Phys. **1**, 20 (2018).

[41] A. P. Luo, Z. C. Luo, H. Liu, X. W. Zheng, Q. Y. Ning, N. Zhao, W. C. Chen, and W. C. Xu, Noise-like pulse trapping in a figure-eight fiber laser, Opt. Express **23**, 10421 (2015).

[42] A. R. Osborne, *Nonlinear Ocean Wave and the Inverse Scattering Transform* (Academic Press, London, 2002).

[43] J. Denschlag, J. E. Simsarian, D. L. Feder, C. W. Clark, L. A. Collins, J. Cubizolles, L. Deng, E. W. Hagley, K. Helmerson, W. P. Reinhardt, S. L. Rolston, B. I. Schneider, and W. D. Phillips, Generating solitons by phase engineering of a Bose-Einstein condensate, Science **287**, 97 (2000).